



An Experimental and Analytical Investigation of Flange Forming By Spinning Process

Mohamed S. Elmasry^{1*}, Hammad T. Elmetwally², Mohamed N. El-Sheikh², Ragab K. Abdel-Magied¹

¹ Mechanical Engineering Department, Faculty of Engineering, Beni-Suef University, Beni-Suef, Egypt

² Production Technology Department, Faculty of Industrial Education, Beni-Suef University, Beni-Suef, Egypt

Article info:

Received: 00/00/2000
Accepted: 00/00/2018
Online: 00/00/2018

Abstract

The Tube flange is typically performed using welding, forging methods, which cost effort and time. In the present work, a metal spinning process to form tube flange was proposed. A flange-forming tool was developed based on the outer tube diameter to form the flange. It consists of three components namely; collet, mandrill, and roller. An experimental work was conducted to investigate the process parameters of the flange process of lead tubes. Different working conditions are considered during conducting of flanged specimens, e.g. rotating speed (rpm), feed rate (mm/rev), and tube wall thickness (mm). The effects of the working conditions on the flanging loads were investigated. The results reveal that the flanging load increases with the increasing rotational speed, tube wall thickness, and with both lower and higher values of feed rate while it decreases with medium values of feed rates. To show the effect of the working conditions on the flange characteristics, a parametric study was conducted. The results show that the surface hardness and surface roughness of the formed flange is improved with increasing all working conditions. A theoretical analysis to model the flange forming loads (axial, radial and tangential) was presented. A comparison between forming loads analytically and experimentally was discussed. This comparison indicates that this percentage of error up to 4% occurs, instead of error percentage up to 28%, in case of neglecting the low feed rate.

Keywords:

Flange process,
Metal tubes,
Flanging ratio,
Forming load,

Nomenclature

A_o Contact area, mm².
 A_t Total cone area.
 D_{tools} The small diameter of the tool.
 $D_{inst\ to}$ Outside tool diameter at the
 D_o Outside tube diameter, mm.
 l_{inst} The length of the slanted part of the flange
 L_f The initial length of forming part.

R_f Outside tube radius g, mm.
 R_1 Inner tube radius, mm.
 S_v feed rate, mm/rev.
 T_{in} Initial Tube thickness before forming mm.
 D_{inst} The tube diameter has the maximum contact area.
 F_Z Tangential component , kN

*Corresponding author

Email address: mms.elmasry@gmail.com

F_Y	Radial component, kN
F_X	Axial component, kN
F	Forming load, kN
h_{tool}	Small diameter of the tool.
T_f	Final Tube thickness after forming mm.
t_{inst}	Initial Tube thickness after forming mm.
V_{inst}	Instantaneous Tube thickness during the forming mm.
V_{in}	The initial volume of the workpiece mm ³ .
ϕ	Half Tool angle.

1. Introduction

Flanged tubes are used in tube lines for the transportation of crude oil, natural gas as well as the other industrial applications; these lines consist of several tubes that are joined together. Many ways to join tubes; e.g., welding, clamped joint, union joint, nosing, flaring and flanges are used. One important method that used to join these tubes is a flange, whereas it keeps the axiality of the tube line assembly and easy to be tightened.

Several techniques have been used to flange tube end. A multi-step upsetting technique has been developed by Hu and Wang [1] to obtain a thick flange. The process has been simulated using the FEM code DEFORM, the simulation results are investigated with discussion of the method of determining the step length. Isaevich et.al. [2] Used punch and die technique to form tube flange. A deforming force in shaping the flange of a tubular workpiece has been calculated. The stresses during the experiments have been investigated. The axial rotary forging process for producing a flange and other parts from tube blanks on machines has been studied by Leonid et.al. [3], in which they concluded that the possibility of rotary forging is restricted due to stability loss in tube blanks which occurs during forming of thick ad wide flanges. Zhongjin et.al. [4] Discussed, in detail, the cold upsetting extrusion process of a tube flange. A FEM simulation, 2D DEFORM program were used to investigate the effect of the tube dimensions and interface friction on the material flow and the cause of forming defects.

Cao et al [5] developed a new incremental sheet forming (ISF) flanging tool as a proposed processing method. A comparative study is carried out by conducting a hole flanging tests.

both of ISF conventional ball nose tool and the new flanging tool are used to evaluate deformation behavior the quality of the final part. A numerical simulation and analytical approach were used to investigate stress-strain distribution. Experiments have been carried out to verify analytical and simulation results.

Hole flange is considered one of the new flange production techniques that using single point incremental forming (SPIF). In which a sheet, with a concentric precut hole and the outer periphery rigidly fixed by a blank holder, is gradually compulsory with a tool to manufacture cylindrical or conical smooth flanges [6-11].

Another investigation of the ability of SPIF process to perform hole flanges in a single stage has been conducted by Borrego et. al. [12] to introduce a better understanding of sheet formability in this demanding situation. Several experimental tests are conducted for AA7075-O metal sheets to evaluate the limiting forming ratio.

Several research works have investigated the flange forming mechanism, the effects of upward and downward burr orientation flange forming directions and the analysis of the direct penetration and re-penetration in the hole flanging process. The analysis of the failure's types, e.g. necking and cracks, that appear under different process conditions have been performed [13- 19].

In this decade, novel spinning processes are being developed which challenges the limitation of traditional spinning technology being used for manufacturing axisymmetric, circular cross-section, and uniform wall thickness parts [20-28]. An optimum spinning process for manufacturing integrated stub end keeping with the dimensions presented in the code has been developed. In which a suitable multi-step spinning process and rollers that can set required shapes and dimensions at each location of the component have been designed by simulation. Hardness has been measured to predict the strength of flanged part [29]. A new process with empirical model has been presented by Hess et.al. [30] to investigate the flange geometry of surface roughness after a friction spinning process. In which the thermomechanical elements of the friction welding process and conventional metal spinning

process are combined. Parameters such as rpm, feed, head radius, and tool infeed width are considered to lead to a measurable surface of the component, as classifier, a gradient boosting machine has been used to predict the valid areas of the design space.

El-Sheikh et al [31, 32] investigated the effect of plug cone angle, tube wall thickness, and tube length on the flanging ratio, surface roughness and surface hardness of the generated widened tube ends. El sheik [33] has developed a new flanging technique, in which a special spinning flange roller is aided with a flange supporting and sizing roller of constant pressure to assist the preventing bending and cracking of the deforming flange. The effect of process parameters on the limiting flanging ratio (LFR), soundness of the generated flange and flanging loads has been investigated. A theoretical analysis has been carried out estimating the flanging loads. Fouly et. al.[34] carried out a flange forming of Al tubes using a ball-shaped tool. A calculation of contact area has been discussed, to investigate the calculated loads. The relation between flanging ratio and thickness has been discussed.

From literature review, it seems that the generality of the published work on flanging processes adopt the techniques of forging (die and punch) or welding, whose operation costs effort and time. Conversely, this work adopts a metal spinning technique with developed flange-forming tool to form the flange. Clearly, the proposed method with the developed tool would have an apparent advantage in the process time and cost reduction. Moreover, the flange characteristics and soundness are improved.

This work presents the possibility of a flanging tube by a spinning process using a developed tool hold at center lathe machine. The design of the developed tool (collet, mandrill, and roller) is based on the outer tube diameter. An experimental work was conducted to form tube flange, from lead metal as received. Different working conditions, i.e., feed rate (S_v), 0.3, 0.4 and 0.5 mm/rev, rotating speed (N), 76, 150, 230 and 305 rpm and thickens 4, 5 and 6 mm is considered. The flanging process for all specimens was conducted at different working conditions. The parametric study is presented to demonstrate the working conditions effect on the flanging load, wall-thickness variation,

Vickers hardness, surface roughness, and flanging ratio. A theoretical analysis to model the flange forming loads (axial, radial and tangential) and its comparison with experimentally measured load are discussed.

2. Experimental work

2.1 Experimental Material

In this work, the material of workpiece was lead (as received), Table (1) depicts its mechanical properties. The tube dimensions were length (L_o) and outer diameter (D_o) of 75 and 84 mm respectively, with different wall thicknesses (T).

Table 1: Mechanical properties of lead (specimen material)

Yield-stress σ_y (N/mm ²)	UTS σ_{Max} (N/mm ²)	Strength coefficient K (MPa)	Strain hardening exponent n
63.95	70.21	36	0.53

2.2 Experimental Setup

In this work, the flanging process is conducted using a flange-forming tool which its design was based on the outer tube diameter. A forming process and tool component (collet, mandrill, and roller) is shown in Fig. (1).

A conventional lathe machine was used to carry out the flanging experiments. Lathe motor is 10 HP, the rotational speed ranges from 12 to 1200 rpm and the feed rate is up to 1.5 mm/rev.

Fig. (2) Illustrates the set of an experiment, to form a flange, the mandrill is inserted into the workpiece, for the sake of dent prevention, and interfered together with the collet. The set of the specimen with tool components is fixed from one end by the lathe chuck, and another end is free. The roller was contracted in the groove of ball bearing that was existing in the housing. Once the roller is engaged with the workpiece, it is rotated. A dynamometer device was joined with the flange-forming roller set to measure flanging loads. The set of the flange-forming roller is inclined with an angle of 35° to the longitudinal axis of the tube. This set moves axially until mid of forming a length of specimen approximately and touch it. The specimen free end was flanged by a spinning

process. The flange forming roller rotated, during flanging process, and moved radially perpendicular to the axial axis of the workpiece. During one stroke, the flange was formed to the flange diameter required. To reduce the friction between flanging forming roller and workpiece, a lubricant oil was used. piece to decrease the generated heat and improve the quality of the formed flange as well.

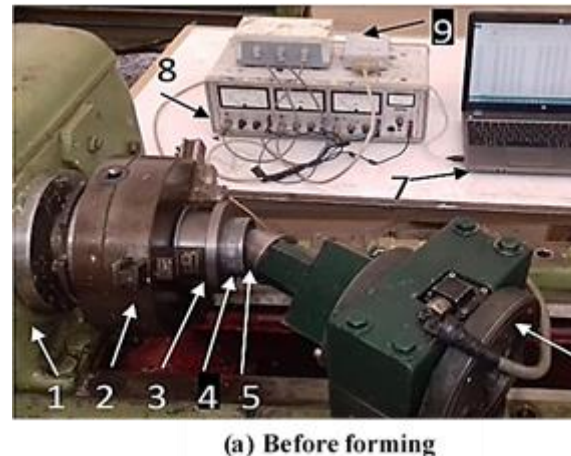


Fig. 1. Developed forming process and tool

2.2. Flange Forming Procedures.

The flanging process is conducted as following steps:

1. The set of flanging forming roller moves axially to the specimen free-end until stopper, and radially until touches tube wall.
2. The flange forming roller moves radially with definite rotating speed (N) and feed rate (S_v) to produce flange width in one stroke, the flange forming roller becomes far from the flange at the end of the forming stroke.
3. The set of the flange forming roller returns to the beginning location



(a) Before forming



(b) After forming

- 1- Gearbox
- 2- Chuck
- 3- Collet
- 4-Specimen (tube)
- 5- Roller (tool)
- 6- Dynamometer device
- 7- Computer device
- 8- Transducer
- 9- Datalogger

Fig. 2. Flanging process (before and after forming) with a set of flanging loads measuring.

4. Another specimen with a new working conditions is switched with the above-mentioned steps. Working conditions were shown in Table 2 and Fig.3

Table 2. Working conditions

Rotational speed, rpm	305, 230, 150, 76
Feed rate (S_v) mm/rev	0.4, 0.3, 0.2
Thicknesses (T) mm	4, 5, 6

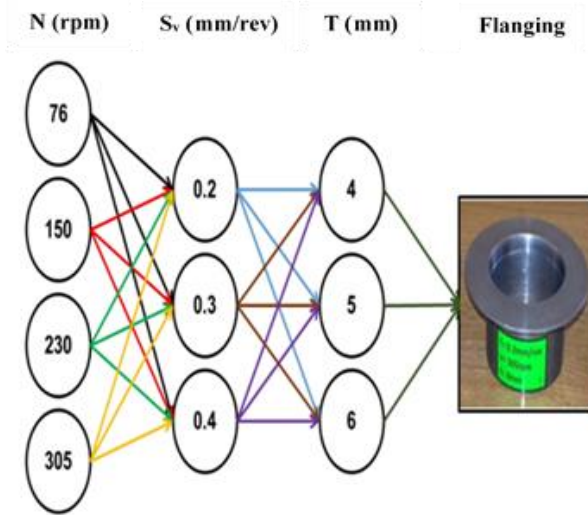


Fig.3. Experimental working conditions arrangement.

2.3 Experimental measurements and tests

In this research, several tests were carried out to study the working conditions effect on the loads and flange characteristics. The flanging loads components (radial, tangential, and axial) that acting upon the flanged part, as illustrated in Fig. (4), were measured at different working conditions. Referred to Fig. (2), the dynamometer was connected to a transducer which transfer output signals to volt to deliver it to data logger that was joined with a computer Pico log program. The load's data were interpreted and converted into KN. Also, a microhardness test was conducted to investigate the working conditions effect on the produced flange hardenability. The hardness was measured along the flange length for sake of determining the metal hardening of the produced flange. Furthermore, the variation in thickness was measured, using a digital camera with high-resolution up to 20 M Pixel in which the flange thickness is calculated based on the pixels of the flange photography to determine either thinning, and thickening occurs. Also, surface roughness occurs due to the flanging tool contact with the workpiece. A surface roughness test was conducted, using the surface device, to check the surface roughness of the flange at different working conditions. The roughness was measured along the flange length in different positions at flange

circumference. Finally, a flange ratio (D_f/D_o) has been measured using a digital micrometer to study the working conditions effect on it, where D_f and D_o are flange and outside tube diameter respectively.

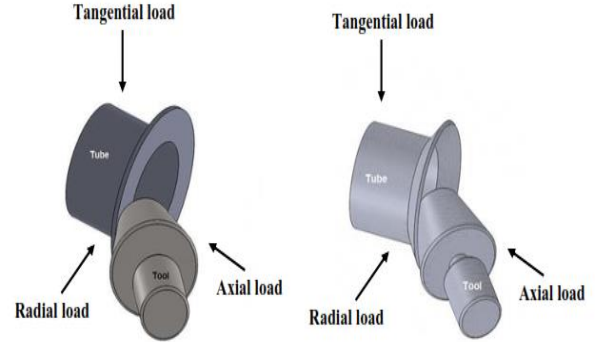


Fig.4. Flanging forming load components.

2.3.1 Analysis of flanging loads

In the theoretical analysis, the flange rotary upsetting is assumed to be a simple case, while the element of material under plane strain is considered upsetting state. The tangential force component on the roller, as well as the axial force component, was obtained explicitly. Figure (4), shows the deformation of the flanges in rotary upsetting with initial tubes thickness (t) and the inner tube radius R_1 . The influential normal force on the contact area (A) between the tube wall and flanging roller is calculated by Eqs. (1-3).

$$F = \sigma A \quad (1)$$

$$\sigma = K \epsilon^n \quad (2)$$

Where

$$\epsilon = \frac{2}{\sqrt{3}} \epsilon_r, \quad \epsilon_r = Ln \frac{R_f}{R_1} \quad \text{and} \quad R_f = x + R_1 \quad (3)$$

For determining the contact area through the indentation phase, it is assumed that the displaced material motion causes only a little change in the overall specimen geometry other than the top surface contouring.

Once this assumption was made, the problem becomes simply upsetting analysis, the bounds of the plane being specified by the rollers and tube diameters.

Fig. (5) presents a possible contour of the contact area boundary between the upset tube and the rotary flanging roller

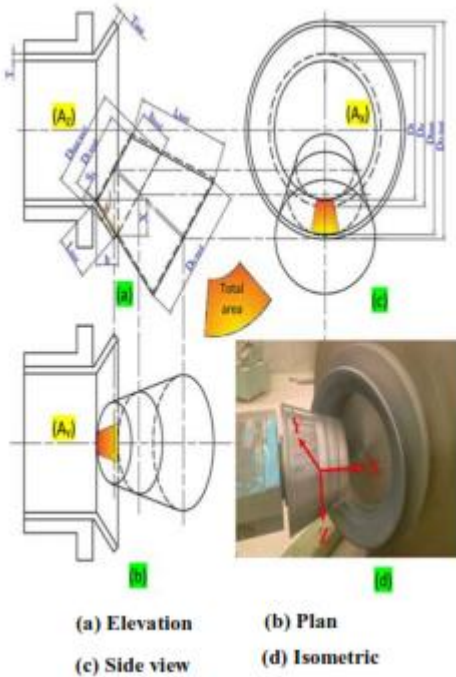


Fig. 5. Schematic of three components of the project area.

Referring to this figure, the projected areas in three directions of the segment between the roller and the specimen can be computed as follows Eqs. (4-11).

According to the constant volume concept volume of the workpiece, and

$$V_{in} = V_{inst} \quad (4)$$

Where V_{in} and V_{inst} are the initial and instantaneous volume of the workpiece (mm³) respectively during the flange forming process (mm³).

$$\frac{\pi}{4} (D_o^2 - D_i^2) L_f = \frac{\pi}{12} h \left[(D_o^2 + (D_i + 2h \tan \theta + 2t_{inst})^2 + D_o * (D_i + 2ht_{inst} + 2t_{inst})) - \left(D_i^2 + (D_i + 2h \tan \theta)^2 + \right) \right] \quad (5)$$

Where D_o is outside tube diameter (mm), D_i is inner tube diameter (mm), L_f is the initial length of forming part (mm), h is the instantaneous length of forming part (mm), θ is angle inclination tool with the tube center and t_{inst} is instantaneous tube thickness during the forming (mm).

$$\frac{\pi}{4} (D_o^2 - D_i^2) L_f = \frac{\pi}{12} h \left[D_o^2 + (D_i + 2h \tan \theta + 2t_{inst}) \left((D_i + 2ht_{inst} + 2t_{inst}) + D_o \right) - D_i^2 + (D_i + 2h \tan \theta) \left((D_i + 2h \tan \theta) + D_i \right) \right] \quad (6)$$

Assume the term value of $(D_i + 2h \tan \theta) = m$, substitute about m in the equation (6), and divide both sides of deduced equation by $(D_o^2 - D_i^2)$

$$3L_f = h \left[1 + \frac{m(2t_{inst} + D_o - D_i)}{(D_o^2 - D_i^2)} \right] \quad (7)$$

Substitute about (m) in equation (14) then

$$2h^2 \tan \theta \left(\frac{(2t_{inst} + D_o - D_i)}{(D_o^2 - D_i^2)} \right) + h \left[1 + D_i \left(\frac{(2t_{inst} + D_o - D_i)}{(D_o^2 - D_i^2)} \right) \right] - 3L_f = 0 \quad (8)$$

From public law

$$h = \frac{-b \pm \sqrt{b^2 - 4ac}}{2a} \quad (9)$$

where $a = 2 \tan \theta \left(\frac{(2t_{inst} + D_o - D_i)}{(D_o^2 - D_i^2)} \right)$,

$$b = \left[1 + D_i \left(\frac{(2t_{inst} + D_o - D_i)}{(D_o^2 - D_i^2)} \right) \right]$$

$$c = -3L_f$$

the final diameter of the specimen at maximum contact area is calculated as follows:

$$x = h \tan \theta \quad (10)$$

$$D_{inst} = D_i + 2x = D_i + 2h \tan \theta \quad (11)$$

Where x is half the distance between D_{inst} and i , D_{inst} is the tube diameter has the maximum contact area.

Calculate the instantaneous tube thickness during the forming Eqs. (12-13).

$$t_{inst} = \frac{T_{in} + T_f}{2} \quad (12)$$

$$t_{inst} = 0.9T_{in} \quad (13)$$

Where T_f is the final tube thickness after forming.

Calculate the final diameter of the cone (tool) at the maximum contact area by Eqs. (14-17).

$$l_{inst} = \frac{h_{tool}}{\cos \phi} \quad (14)$$

$$h_{tool} = l_{inst} * \cos \phi \quad (15)$$

$$y = l_{inst} * \sin \phi \quad (16)$$

$$D_{inst \ tool} = D_{tool \ s} + 2y \quad (17)$$

Where l_{inst} is the length of the slanted part of the flange during forming, h_{tool} is height between the small diameter of the tool and the

instantaneous diameter at the contact area, ϕ is half tool angle, y is the distance corresponding to the angle (ϕ), $D_{inst\ tool}$ is outside tool diameter at the contact area of the flange during forming and $D_{tool\ s}$ is small diameter of the tool.

The tool angle that contact with the specimen is calculated as follows Eqs. (18-19):

$$\cos \alpha = \frac{R-S_v}{R} \quad (18)$$

$$\alpha = \cos^{-1} \frac{R-S_v}{R} \quad (19)$$

Where α cone angle at the contact area, R is a large radius of cone (tool) and S_v feed rate (mm/rev).

Calculate the cone area by Eqs. (20-23).

$$A_{tc} = \pi(R - r)\sqrt{(R - r)^2 + h_{tool}^2} \quad (20)$$

Where A_{tc} is a total cone area and r small radius of cone.

$$\text{Contact area} = \frac{\text{Total cone area} \cdot \alpha}{360} \quad (21)$$

$$A = \frac{A_{tc} \cdot \alpha}{360} \quad (22)$$

By substitute in Equation 1, the deformation loads can be calculated as follows:

F =

$$k \left(\frac{2}{\sqrt{3}} \right) \ln \left(\frac{\left[- \left[1 + D_i \left(\frac{(2+0.9T_{in}+D-D_i)}{(D^2-D_i^2)} \right) \right] + \sqrt{\left[1 + D_i \left(\frac{(2+0.9T_{in}+D-D_i)}{(D^2-D_i^2)} \right) \right]^2 - 4 \left(2 \tan \theta \left(\frac{(2+0.9T_{in}+D-D_i)}{(D^2-D_i^2)} \right) \right) (-3L_f)}{2 \left(2 \tan \theta \left(\frac{(2+0.9T_{in}+D-D_i)}{(D^2-D_i^2)} \right) \right) \cdot \tan \theta} \right] + R_1}{R_1} \right) \quad (23)$$

The required data for calculations are listed in table 3. A comparison between computed results by mathematical model and

experimental results is presented and discussed in the following section.

Table 3. Parameters of calculation of spinning force components.

Parameter	Value
Strength coefficient (K), Mpa	36
Strain hardening exponent (n)	0.53
The initial wall thickness of tube (t), mm	4, 5, 6
workpiece outside radius before forming (R), mm	85
Radial feed rate (S _v), mm/rev	0.2, 0.3, 0.4

3. RESULTS AND DISCUSSIONS

3.1 FLANGING LOADS

The flanging loads mean the deformation load generated due to the forcing of the flanging tool on the tube end to form its flange. The flanging load components are illustrated in a load-displacement diagram as shown in Figure. (6), in which the abscissa y represents the resultant load while the abscissa x represents the flange stroke. The experimental conditions for this example are $T = 4$ mm, $N=76$ rpm, and $S_v=0.3$ mm/ rev. It could be seen that there is an incremental increasing in radial load from the beginning until it becomes maximum in the middle of x -axis approximately, and then it decreases gradually to the end of flanging process. This is referred to the contact area between flanging tool and specimen, i.e., the contact area is small at the beginning of the flanging process then increases gradually to the middle point approximately and decreases again gradually to the end of flanging process. Conversely, the axial and tangential loads have gradual decreasing from the starting of the forming stroke until becomes minimum in the middle of x -axis approximately and then it increases gradually to the end of flanging process. Because at the beginning of the flanging process high axial and tangential forces are required to yield the material in the direction of the flanging, also at the end of flanging stroke high axial and tangential forces are required to iron the flange.

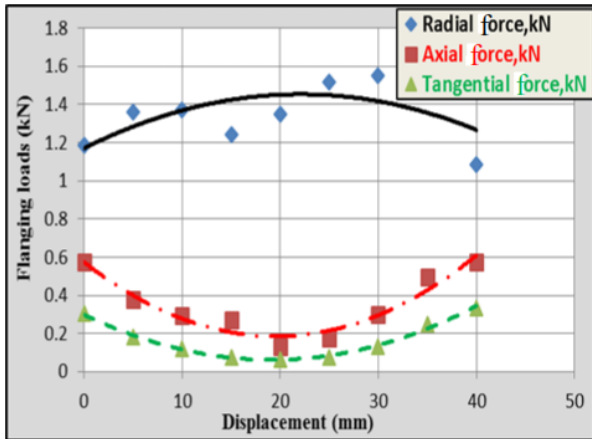
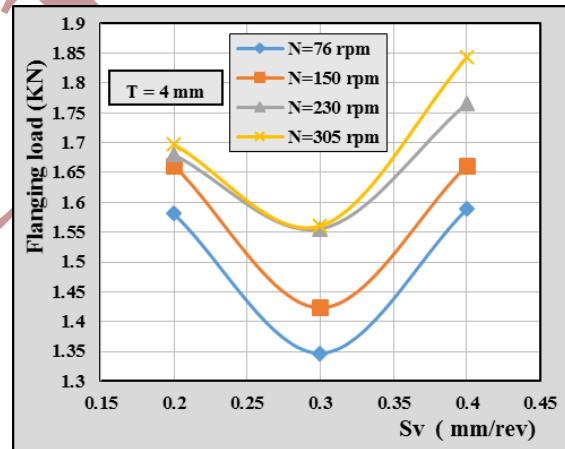


Fig. 6. Loads - displacement diagram ($S_v = 0.3\text{mm/rev}$, $N = 76\text{rpm}$ and $T = 4\text{mm}$).

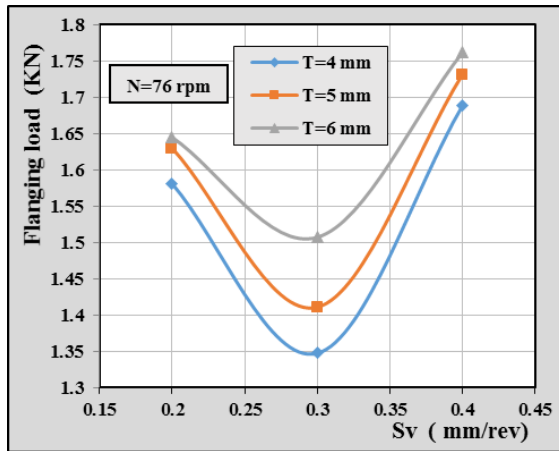
Figure. (7) Depicts the effect of the roller feed rate, (S_v) on the maximum of resultant flanging load. The maximum flanging load is referred to the higher value of the flanging load along flanging process. In this example, the working conditions are $T = 4\text{mm}$ and different N for Figure (7-a) while $N = 76\text{rpm}$ and different values of T as in Figure (7-b). It could be seen from both Figures a and b that the maximum flanging load decreases gradually from the beginning of the process until S_v equals 0.3mm/rev then it turns and increases gradually to the end of the flanging process. It should be noted that the minimum flanging load is at the feed rate of 0.3mm/rev (either at different rotational speeds or different thicknesses in both Figures). This may be referred to the effect of roller rpm on the material flow, i.e., at low feed rate over-rolling occurs which results in work hardening and then need high force. With increasing feed rate, there is a harmony between material flow and feed rate, which tends to decrease in the forming force. At high feed rate, the required load for the flanging increases to force the material flow to be formed through the forming stroke. It should be noted that this analysis indicates that the optimum and recommended feed rate is 0.3mm/rev .

Evidently, it can be seen from both Fig. 7 (a and b) that the flanging load increases with increasing both rotational speed and tube

thickness. i.e., fig (7- a) shows that the rotational speed has an effect on the flanging load with a constant thickness. Since the flanging load raises, this resulted from the surface hardening that has occurred on the workpiece; i.e. the rpm increasing tends to excess passes on the particles of workpiece surface. Therefore, it becomes very hard and needs a higher forming force. Also, fig. (7-b) illustrates the increase in flanging load with increasing tube thickness because the volume of the material has to be formed increases with increasing material thickness which leads to needing a high forming force. Evidentially, from this figure, it could be seen that the minimum force could be obtained at working conditions ($S_v = 0.3\text{mm/rev}$, $N = 76\text{rpm}$ and $T = 4\text{mm}$) which are considered as recommended values of these parameters to optimize flanging load.



(a) Different rotational speed; $T=4\text{mm}$



(b) Different tube wall thickness; N = 76rpm.

Fig. 7. Effect of feed rate on the maximum flanging load.

Fig. (8) presents a comparison between the theoretical and experimental results of flanging loads. It could be seen that the error between the theoretical and experimental values ranges from 1 to 28 %. This may be referred to the changing in feed rates, i.e., at low feeding rates; there is a considerable difference between the experimental and theoretical results because the surface hardening of the metal occurs, during the process, due to the extra rotation on the surface particle, which leads to increasing the surface hardening. At medium and high feeding rates there is a very high correlation between theoretical and experimental results because it does not happen surface hardening of the metal during the flanging process. This error ranges from 1 to 4% in case of neglecting the low feed rate because of the surface hardening explained above.

3.2 Limiting Flanging Ratio (LFR)

Fig. (9) It depicts the effect of the roller feed rate, (S_v) on the limiting flanging ratio (LFR). The LFR is defined as the maximum limit of flange diameter to tube outer diameter ratio

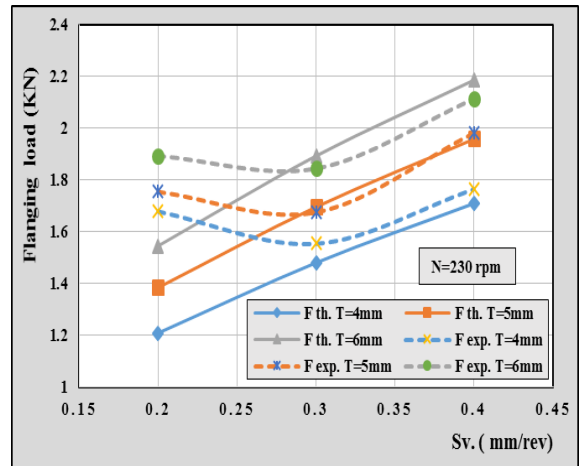
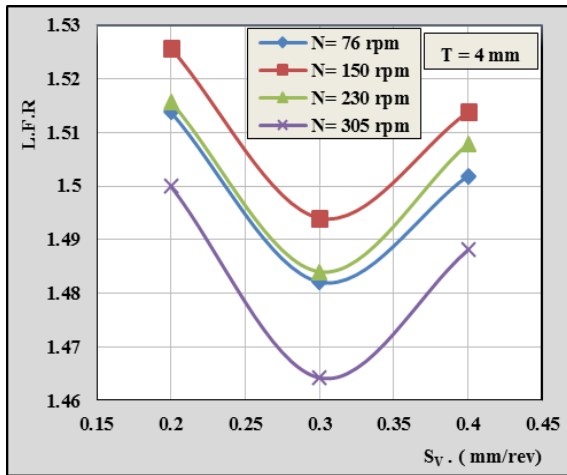


Fig. 8. Comparison between theoretical and experimental flanging loads

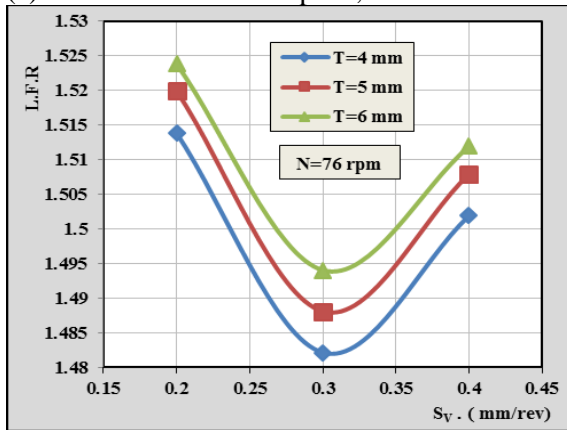
A digital micrometer was used to measure the produced flange. The experiment working conditions in this example are $T = 4$ mm and different N as in Fig. (9-a) while $n = 76$ mm/rev with different values of T as in fig (9-b). It could be seen from both (fig. 9-a & 9-b) that the behavior or trend of (LFR) is the same as the flanging load at the same parameters and experimental conditions. i.e., a gradual decrease occurs from the beginning of the process until S_v equals 0.3 mm/ rev then it turns with gradual increase to process end. It should be noted that the minimum LFR also occurs at the feed rate of 0.3 mm/rev (either at different rotational speeds or different thicknesses in both figures). Which confirm the dependency of LFR on the flanging force.

Practically, it is known that the recommended flanging ratio FR about 1.4, which could be obtained in this study at all working conditions. It should be noted that these values could be recommended for these parameters to produce practical FR. This is because of the limiting flanging ratio (LFR) practically rapprochement 1.5.

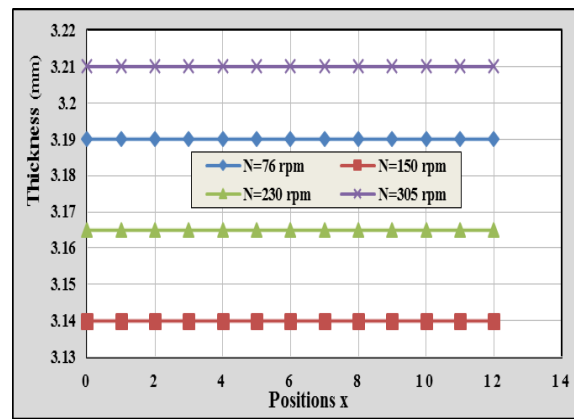
It should be noted that the limits of flanging ratio depend on the reduction in flange thickness, i.e. when the LFR reached 1.5 , the reduction in thickness was less than 20% but at LFR about 2.5, the reduction in thickness was more than 80%.



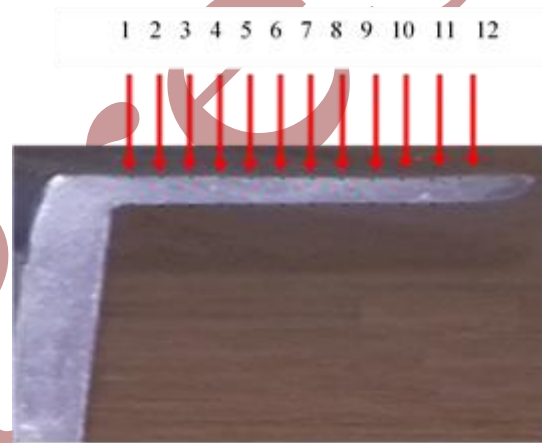
(a) Different rotational speed; $T=4$ mm



(b) Different tube wall thickness; $N=76$ rpm



(a)



(b)

Fig 9. Effect of feed rate on the limiting flanging ratio (LFR).

3.3 Thickness Variation

Fig. (10) illustrates the thickness variation (T) along the flange at different values of rotational speed (N), feed ($S_v = 0.3$). The x -axis, in this figure, refers to the different positions (1 to 12) over the flange length from the tube wall to free side as shown in Fig. (10). It can be seen that a little rise in the flange thickness, seems to be constant approximately, over the flange length because the flange is exposed to ironing process during the flange forming which keeps the thickness in equal distribution. But on the other hand, the flange thickness is affected by rotational speed, and the minimum reduction in thickness occurs at N equal 305 rpm, which is more consistency with recommended parameters to obtain the flange ratio as mentioned previously.

Fig. 10. Thickness variation over the flanging length ($T = 4$ mm and $S_v = 0.3$ mm/rev).

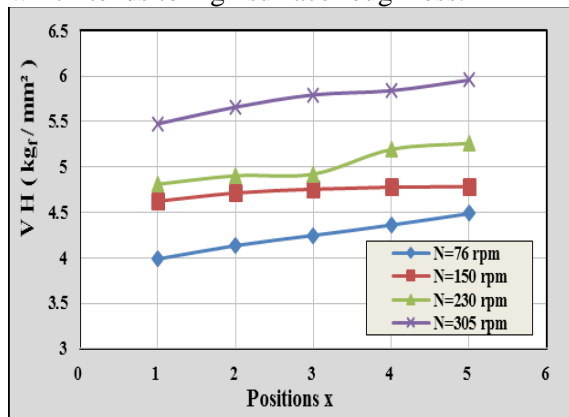
3.4 Hardness of flange surface

Fig. (11) Shows the flange surface variation as a function of the rpm. The X -axis, in this figure, refers to the various positions (1 to 5) over the flange length from the tube wall to flange end. In this example, the working conditions are $T = 4$ mm, $S_v = 0.30$ mm/rev, and different rotational speeds. It could be known that the hardness measured overall positions were larger than the hardness of the received material due to work hardening. From the figure, it can be seen that the surface hardness increases gradually from the tube wall to the free side of the flange. This is due to the standing contact between the tool and free side of flange from the start of the flanging process with the increasing incrementally to the end of the process; this continuous incremental contact increases the surface hardening gradually.

Furthermore, the hardness of the flange surface over the flange length increases due to increase in rpm, because excess rotations on the particles of the formed part causes the hardening in workpiece surface.

3.5 Surface roughness of the flange

Fig. (12) Shows the relation between feed rates and the waviness variation of the flange surface measured in μm . In this example, the working conditions are $T=4\text{ mm}$, and different rotational speeds. In this figure the surface roughness increases incrementally from the tube wall to the free side of the flange. Because with increasing feed rate, more vibrations occur, this incremental vibration increases the surface roughness gradually. Moreover, as the rpm increases, the surface roughness of the flange increases over the flange length, because the more rpm the high vibrations also occur, which tends to high surface roughness.



(a)



(b)

Fig. 11. Micro-hardness over the flange length ($T = 4\text{ mm}$, $S_v = 0.3\text{ mm/rev}$)

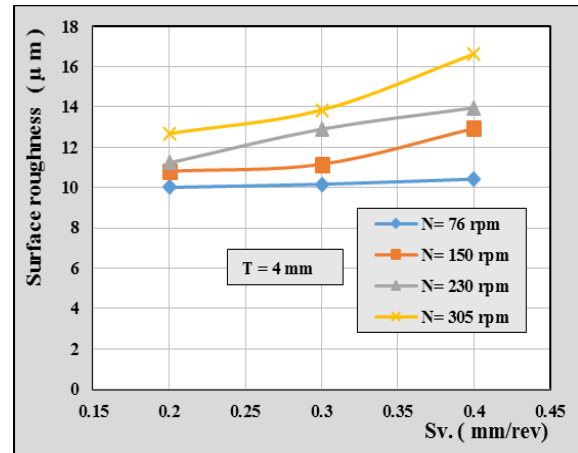


Fig. 12. Effect of feed rate on the surface roughness

Conclusion

A flanging process using the metal spinning technique with a developed flange-forming tool is proposed. Experimental work was conducted for various specimens with different working conditions to form a flange of the lead metal tube. A new finding of this work can be concluded as follows:

- Along the formed flange, the thickness is uniform, but it varied with different working conditions. Conversely, the surface hardness increases gradually from inner to outer diameter of the formed flange with all working conditions. Surface roughness increases with increasing all working conditions along the formed flange.
- The limiting flanging ratio increases with medium values of rotational speed and both of low and high feed rate, conversely, it decreases with both of low and high rotational speed and medium values of feed rates.
- The flanging load affected by working conditions. The flanging load increases as rpm increases and wall tube thickness, while it decreases with medium values of feed rates and increases with both of low and high feed rate.
- An analytical flanging loads formula was derived. A good agreement between the deducted forces analytically and that measured experimentally were found. A little error ranges from 1 to 4% could exist instead of 1 % to 28% in case of neglecting the low feed rate because of the surface hardening explained above.

References

- [1] X.L. Hu and Z.R. Wang, "Numerical simulation and experimental study on the multi-step upsetting of a thick and wide flange on the end of a pipe", *Journal of Materials Processing Technology*, Vol. 151, pp. 321–327, (2004).
- [2] L. A. Isaevich, M. I. Sidorenko, and V. A. Gurinovich, "Calculating the Deforming Force in Shaping the Flange of a Tubular Workpiece", *Russian Engineering Research*, Vol. 27, No. 5, pp. 275–278, (2008).
- [3] L.B. Aksenov and S. N., Kunkin *Metal Flow Control at Processes of Cold Axial Rotary Forging 2nd ed.*, Springer, New York, pp. 62–75, (2016).
- [4] Z. Wang, and J. Lu, Z.R. Wang, "Numerical and experimental research of the cold upsetting-extruding of tube flanges" *Journal of Materials Processing Technology*, Vol.110, pp.28-35, (2001).
- [5] T. Cao, Bin Lu, H. Ou, H. Long, J. Chen "Investigation on a new hole-flanging approach by incremental sheet forming through a featured tool" *International Journal of Machine Tools & Manufacture* 110 (2016) 1-7.
- [6] Q. Lin, W.Dong, Z.Wang, and K. Hirasawa, "A new hole-flanging method for thick plate by upsetting process," *Trans. Nonferrous Met. Soc. China*, Vol.24, pp. 2387–2392, (2014).
- [7] V. Cristino, L. Montanari, M.B. Silva, A.G. Atkins, and P.A.F. Martins, "Fracture in hole-flanging produced by single point incremental forming", *International Journal of Mechanical Sciences*, Vol.83 1, pp.46-154, (2014).
- [8] M. Borrego, D. Morales-Palma, A. J. Martinez-Donaire, G. Centeno, and C. Vallellano, "On the study of the single-stage hole-flanging process by SPIF" *Procardia Engineering*, Vol. 132 pp. 290 – 297, (2015).
- [9] T. Kumagai and Hiroyuki Saiki, "Deformation Analysis of Hole Flanging with Ironing of Thick Sheet Metals" *Metals and materials*, Vol. 4, No. 4, pp. 711-714. (1998).
- [10] E. Haghani, A. Gheysarian and M. Honarpisheh "Design and manufacture a novel tool in the incremental sheet metal forming process and its effects on the process parameters", *Journal of Computational and Applied Research in Mechanical Engineering*, in press. Vol.8, No.2, pp.121-132, (2018).
- [11] A. Gheysarian, and M. Honarpisheh, "An experimental study on the process parameters of incremental forming of Al-Cu bimetal", *Journal of Computational and Applied Research in Mechanical Engineering*, Vol. 7. No. 1, pp. 73-83, (2017).
- [12] M. Borrego, D. Morales-Palma, A. J. Martinez-Donaire, G. Centeno, C. Vallellano "On the study of the single-stage hole-flanging process by SPIF" *Procedia Engineering*, Vol. 132. No. 1, pp. 290 – 297, (2015).
- [13] S. Thipprakmas and W. Phanitwong, "Finite element analysis of flange-forming direction in the whole flanging process", *Into. J. Adv. Manu. Techno*, Vol.61, pp.609–620, (2012).
- [14] G. Hussain, H. Valaei, Khalid A. Al-Ghamdi, and B. Khan "Finite element and experimental analyses of cylindrical hole flanging in incremental forming", *Journal of Materials Processing Technology* Vol.26, pp.2419–2425, (2016).
- [15] Y.-M. Huang and K.-H. Chien, "Influence of Cone Semi-Angle on the Formability Limitation of the Hole-Flanging Process", *Into. J. Adv. Manu. Techno* Vol.19, pp.597–606, (2002).
- [16] A. Kacem, A. Krichen, P.Y. Manach, S. Thuillier, and J.W. Yoon, "Failure prediction in the hole-flanging process of aluminum alloys," *Engineering Fracture Mechanics* Vol.99, pp.251–265, (2013).
- [17] H. Soussi, N. Masmoudi, and A Krichen, "Analysis of geometrical parameters and occurrence of defects in the hole-flanging process on thin sheet metal", *Journal of*

- Materials Processing Technology, Vol.3 ,No.2,pp.22-34,(2015). .
- [18] A. Kacem, A. Krichen, and P. Manach, "Occurrence and effect of ironing in the hole-flanging process," *Journal of Materials Processing Technology*, Vol. 211 pp.1606–1613,(2011).
- [19] Gh. Payganeh ,and J. Shahbazi Karami and K. Malekzadeh Fard , "Finite element comparison of single, bi-layered and three-layered tube hydroforming processes", *Journal of Computational and Applied Research in Mechanical Engineering*, Vol. 2. No. 2, pp. 96-80, (2013).
- [20] O. Music, and J.M. Allwood, K. Kawai, "A review of the mechanics of metal spinning", *Journal of Materials Processing Technology*, Vol.210 ,pp. 3-23, (2009).
- [21] E. Hagan ,and J. Jeswiet , "A review of conventional and modern single-point sheet metal forming methods, Proceedings of the Institution of Mechanical Engineers, Part B", *Journal of Engineering Manufacture*, Vol.217 ,pp. 213-225, (2003) .
- [22] J. Jeswiet ,and F. Micari G. Hirt, A. Bramley , "Asymmetric single point incremental forming of sheet metal" , *CIRP Annals – Manufacturing Technology* ,Vol.54 ,pp. 623-649, (2005).
- [23] Q.X. Xia , "Investigation on the mechanism of the spinning technology of the 3D Non-axisymmetric parts" , *Chinese Journal of Mechanical Engineering*, Vol.40, pp. 153-156. , (2004).
- [24] B. Awiszus, and F. Meyer , "Metal spinning of non-circular hollow parts" ,in: *Proceedings of the Eighth International Conference on Technology of Plasticity*, October, Verona, Italy, Vol.3,pp. 353-355, (2005).
- [25] B. Awiszus, and S. Hartel , "Numerical simulation of non-circular spinning: a rotationally non-symmetric spinning process" ,*Prod. Eng. Res. Delve*. Vol. 5 ,pp.605-612, (2011).
- [26] D. Schmoeckel and S. Hauk , "Tooling and process control for splitting of disk blank" , Vol.98 pp.65-69, (2000) .
- [27] Q.X. Xia, M.H. Yang, Hu. Y and X.Q. Cheng, "Numerical simulation and experimentation cup-shaped thin-walled inner rectangular gear formed by spinning", *Chinese Journal of Mechanical Engineering* ,Vol.42 ,pp.192-196, (2006).
- [28] C.C. Wong, T.A. Dean, J. Lin "A review of spinning, shear forming and flow forming processes" *International Journal of Machine Tools & Manufacture* 43 (2003) 1419–1435.
- [29] G. Gwak , J. Jeon , J. Cho , J. Choi , and J. Kim, "Development of Integrated Stub End by Spinning Process" ,*International Journal of Precision Engineering and Manufacturing*, Vol. 16, No. 7, pp. 1473-1477 ,(2015).
- [30] S. Hess. B. Lossen, D. Biermann, W. Homberg, and T. Wagner , "Analysis of the surface roughness obtained in a friction spinning process based on empirical models", *Int J Adv Manuf Technol* ,Vol.74,pp.1655–1665, (2014).
- [31] O.I. Ahmed, M.N. El- Sheikh, and A.A. Ibrahim, " An Investigation into Flanging of Tube Ends using Truncated Conical Plugs," *Bulletin of the Faculty of Engineering, Assiut University* ,Vol. 17 ,No.2, (1989).
- [32] M.N. El-Sheikh, A.T. Mohamed, A.A. Ibrahim , "Widening of aluminum tube using conical plugs", *Minia Journal of Engineering and Technology*, Minia University Vol. 9 No. 1, pp. 27-38, (1990).
- [33] M.N El-Sheikh , "An Investigation Into Flange Forming Of Metallic Tubes", *Proceeding of 6th ed., international conference (MDP6), Current Advances in Mechanical Design & Production*, Cairo University, Egypt, (1996).
- [34] M. S. Zein El-Abden, and M. Abdel-Rahman , "A rotary flange forming process on the lathe using a ball-shaped tool" ,*Journal of Materials Processing Technology* ,Vol.170 501–508, (2005).

in Press